Improved efficiency with adaptive front and rear axle independently driven powertrain and disconnect functionality

Transportation Engineering 13 (2023) 100192

Contents lists available at ScienceDirect

Transportation Engineering

journal homepage: www.sciencedirect.com/journal/transportation-engineering

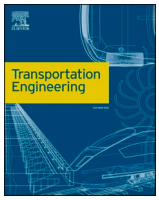

Improved efficiency with adaptive front and rear axle independently driven powertrain and disconnect functionality

Y. Xu [*,a,b], A. Kersten [a,c], S. Klacar [d], B. Ban [e,f], J. Hellsing [a], D. Sedarsky [b]

[a] China Euro Vehicle Technology (CEVT) AB, Göteborg, Sweden
[b] Chalmers University of Technology, Division of Energy Conversion and Propulsion Systems, Mechanics and Maritime Sciences, Göteborg, Sweden
[c] Bundeswehr University Munich, Department of Electrical Engineering, Neubiberg, Germany
[d] Infimotion Technology Europe AB, Göteborg, Sweden
[e] Torquery Consulting, Göteborg, Sweden
[f] University of Zagreb, Faculty of Electrical Engineering and Computing, Department of Electric Machines and Automation, Zagreb, Croatia

ARTICLE INFO

Keywords:
Electric vehicle
Energy efficiency
Dual-motor powertrain
Mechanical disconnect
Mode selection
Dynamic programming

ABSTRACT

Front and rear axle independently driven (FRID) powertrains are becoming a popular solution for electric vehicles (EVs) due to torque distribution capability which can enhance powertrain energy efficiency. Typically, permanent magnet synchronous machines (PMSMs) are used for FRID powertrains due to their high torque, and power density. However, the drive-cycle efficiency of FRID powertrains with PMSMs is typically reduced in comparison to single motor drives. This is due to the unwanted no-load losses of PMSMs in the field weakening region. To overcome this drawback of PMSM FRIDs, this paper proposes an adaptive front- and rear-axle independently driven (AFRID) powertrain, utilizing two dog clutches, so that the powertrain can be operated in different modes (rear, front, and all-wheel drive) by adaptively connecting and disconnecting the front and/or rear electric drive unit (EDU). A rule-based mode selection strategy is developed to utilize the flexibility of different powertrain operating modes of the powertrain for maximizing the energy efficiency of the EDU. The simulation results show that the suggested AFRID powertrain, in comparison to a common FRID powertrain, can improve the WLTC drive-cycle consumption from 22.17 kWhh to 20.50 kWhh per 100 km. Based on the route and road-load information, the energy-saving potential of the AFRID powertrain can be further improved to 20.37 kWhh per 100 km by a suggested predictive mode selection strategy, achieving an optimal mode selection.

1. Introduction

With increasing global climate concerns, battery electric vehicles (BEVs) are showing promise for future mobility due to low equivalent life-cycle CO2 emissions [1,2]. However, with the limitations of current battery energy density, driving range has become a main focus within the automotive industry [3,4]. Efficient electric powertrains that can intelligently mitigate losses and consistently optimize recuperation of energy in real-driving scenarios, are vital for maximizing the driving range in relation to the installed battery capacity [5].

Dual motor powertrains are considered to be a promising alternative to single motor BEV powertrains due to their torque distribution functionality, high power density [6–9]. According to Zheng et al. [10], Hajduga [11], Wang et al. [12], the most common dual-motor coupling configurations can be summarized as follows: front- and rear-axle independently driven by two electric motors, single axle driven by two electric motors coupled via a 2-speed gearbox, and single axle driven by two electric motors coupled via a planetary gearbox. As for example shown in [13] and [14,15], planetary gear based power split system solutions or 2-speed gearbox configurations can improve the powertrain efficiency in comparison to a single motor powertrain. Nevertheless, the FRID powertrain is often chosen by EV manufacturers due to its high performance all-wheel-drive capability and fault-tolerance, while maintaining a reasonable level of cost, space requirement and structural complexity [16–18].

PMSMs are widely used in single motor and FRID powertrains due to their high torque density and compact size, Fig. 1a [19,20]. However, due to the back electromotive force (EMF) generated by the permanent magnets, PMSMs have inevitable no-load losses when operated in the field weakening region [21]. Hence, it is necessary to take the no-load

* Corresponding author.
E-mail address: yuxu@chalmers.se (Y. Xu).

https://doi.org/10.1016/j.treng.2023.100192
Received 17 March 2023; Accepted 12 July 2023
Available online 13 July 2023

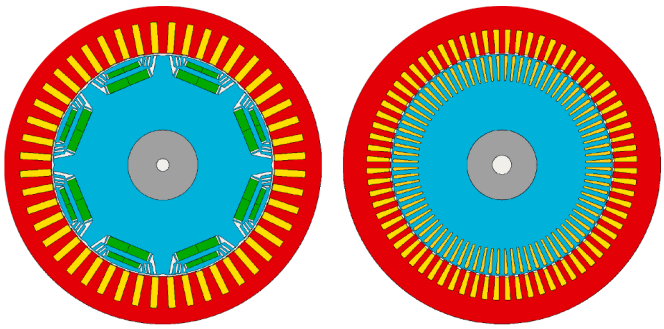

Fig. 1. Example of a (a) permanent magnet synchronous machine (PMSM) and (b) induction machine (IM). Figures are generated from Ansys Motor-CAD.

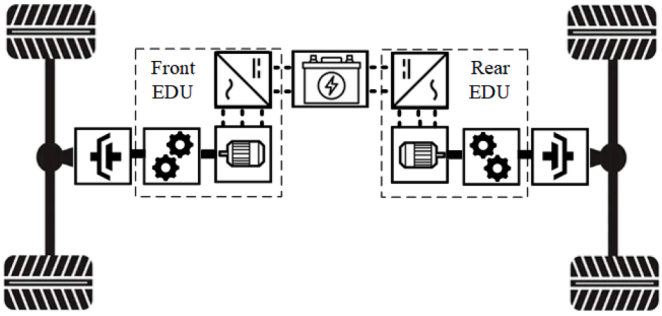

Fig. 2. Typical AFRID powertrain configuration with front- and rear-axle EDUs including dog-clutches. Each EDU consists of a gearbox, a three-phase motor, and an inverter (supplied by the high-voltage propulsion battery).

Table 1
EDU and clutch engagement-states for each operating mode.

	Front EDU	Rear EDU	Front clutch	Rear clutch
FWD	active	inactive	engaged	disengaged
RWD	inactive	active	disengaged	engaged
AWD	active	active	engaged	engaged

Table 2
Vehicle parameters.

Parameter	Symbol	Value	Unit
Vehicle mass	m	2640	kg
Vehicle drag coefficient	C_d	0.372	-
Vehicle frontal area	A	2.8	m^2
Tire rolling radius	R_r	377	mm
Tire rolling resistance	C_r	0.01	-

losses of the PMSMs into consideration when optimizing the operation of a FRID powertrain [22] equipped with PMSMs. Otherwise, the efficiency over a drive cycle of a FRID system can be decreased compared to single motor powertrains [23]. In contrast, induction machines (IMs, Fig. 1b) do not produce back EMF because there are no permanent magnets in the rotor structure. In [24], a FRID powertrain equipped with two identical IMs was investigated based on a numerical motor loss model. The results suggest that under low torque conditions, instead of dual usage, single motor operation is more efficient. In contrast, according to Yuan and Wang [25], it is most efficient to share torque equally between two identical permanent magnet synchronous machines (PMSMs) due to the high idle losses of PMSMs. In [26–28], several power distribution control strategies for FRID powertrains with different motor power ratings are analyzed, improving the drive cycle efficiency in comparison to single-motor powertrains. In addition, simple clutches can be used to intermittently disengage/synchronize one or both PMSMs when operated at low or no-load to increase the powertrain efficiency [29,30]. As quantified in [31] for a FRID powertrain with two different motors with only one added clutch, the drive cycle energy consumption can be reduced by 5% to 6%. A similar improvement is shown in [32] for a city bus with a FRID powertrain utilizing one clutch.

The aforementioned studies have explored effective solutions to reduce the energy consumption of FRID powertrains by either introducing an optimal torque distribution strategy or by eliminating the no-load losses of one PMSM via a clutch. However, to the best knowledge of the authors, no research investigations have been focused on FRID powertrains with two different motors that can be independently disconnected. With such a configuration, FRID powertrains should be able to further utilize the efficiency characteristics of each motor according to different driving conditions. Moreover, the detailed clutch engagement and disengagement processes and corresponding transient energy loss, such as the motor speed control to incorporate clutch engagement and disengagement, are not investigated yet.

To tackle the above research gaps, this study proposes an adaptive front and rear axle independently driven powertrain (AFRID) incorporating two PMSMs with the same power rating but different efficiency characteristics and corresponding (independently actuated) clutches. An EDU speed control procedure which minimizes the energy losses during clutch engagement and disengagement transition when shifting powertrain operating mode is developed. To reveal the full potential of AFRID powertrain with the consideration of transient energy loss during clutch engagement and disengagement, a predictive operating mode selection strategy which utilizes the route information with dynamic programming (DP) optimization algorithm is proposed. The benefit, as compared to a standard rule based strategy, is evaluated and verified under a number of standard driving cycles using simulations (a standard procedure in the automotive industry).

2. Powertrain modeling and control hierarchy

The configuration of the considered AFRID powertrain is shown in Fig. 2. The configuration consists of two EDUs, located at the front and rear drive axles, respectively. Both EDUs can be independently connected and disconnected to the corresponding drive axle via a dog clutch. Depending on the engagement of the EDUs and clutches (summarized in Table 1), AFRID powertrains can shift among three operating modes: front-wheel-drive (FWD), rear-wheel-drive (RWD), and all-wheel-drive (AWD) mode.

2.1. Vehicle longitudinal dynamics

This study only focuses on longitudinal vehicle dynamics. Thus, vehicle handling and vertical vibrations are not considered here. In the longitudinal direction, the force opposing the motion of a vehicle consists of four terms: gradient resistance, aerodynamic resistance, tire rolling resistance, and acceleration contribution. These resistance terms are balanced with the traction torque as follows

$$\overbrace{\frac{T_{dem}}{R_r}}^{\text{Tract. force}} = \overbrace{mg\sin(\theta)}^{\text{Gradient res.}} + \overbrace{\frac{1}{2}\rho_{air}C_dAv^2}^{\text{Aerodyn. drag}} + \overbrace{C_rmg\cos(\theta)}^{\text{Rolling res.}} + \overbrace{(m+m_i)\dot{v}}^{\text{Acc. force}} \quad (1)$$

where T_{dem} is the vehicle torque demand in reference to the wheels, R_r is the tire rolling radius, m is the vehicle mass, g is the gravitational acceleration, θ is the road gradient, ρ_{air} is the air density, C_d is the aerodynamic drag coefficient, A is the vehicle frontal area, v is the vehicle speed, C_r is the tire rolling resistance coefficient, and m_i is the equivalent inertia mass from wheels and the EDU(s) connected to the powertrain.

The vehicle investigated in this study is an E-size SUV. Its main

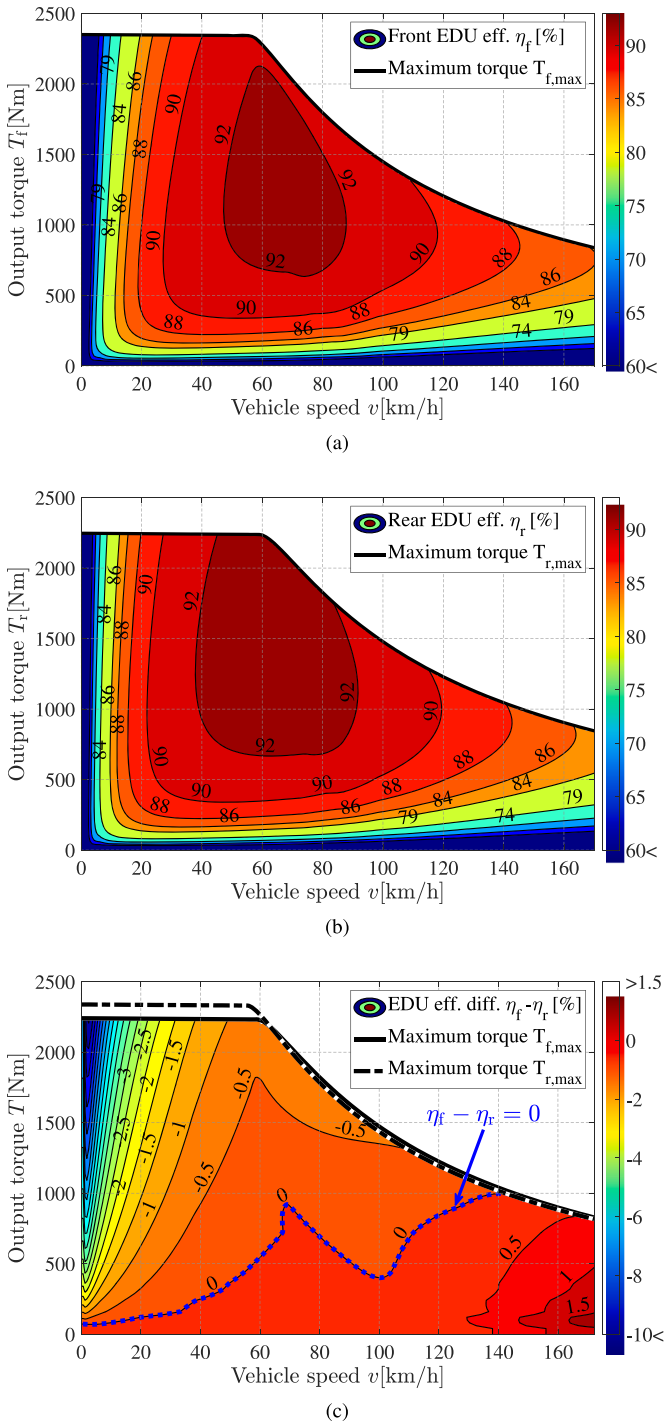

Fig. 3. EDU efficiency map of the (a) front and (b) rear motor, and (c) their corresponding efficiency difference map.

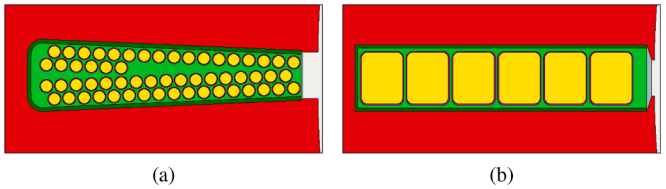

Fig. 4. Example of (a) stranded wire and (b) hairpin electric machine stator winding design. Figures are generated from Ansys Motor-CAD.

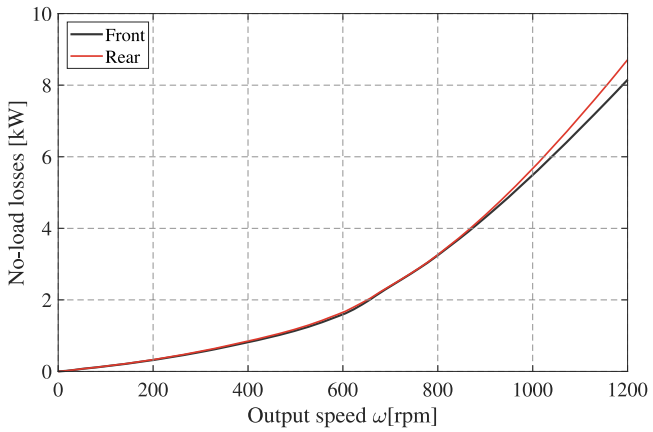

Fig. 5. No-load losses of the front and rear EDU relative to the output speed of the motors.

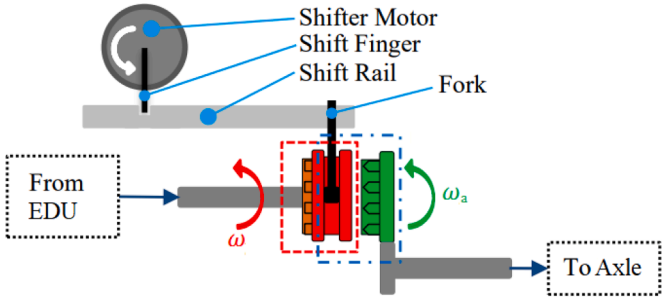

Fig. 6. Structure of dog clutch assembly.

parameters are shown in Table 2.

2.2. Electric drive units

Each EDU consists of an electric motor, an inverter, and a reduction gear. The efficiency maps of the front and rear EDU are shown in Fig. 3a and b, respectively. Both EDUs operate in a similar torque-speed range, which provides FWD, RWD, and AWD capability for the entire speed range of the vehicle. As highlighted in Fig. 3c, the front EDU has higher efficiency at higher speeds and low-torque operation (PMSM with stranded windings Fig. 4a [33,34]), whereas the rear EDU operates more efficiently at lower speeds and high-torque operating conditions (PMSM with hairpin windings Fig. 4b [33,34]). The efficiency differences arise due to conductor shape and size, affecting the eddy current distribution within the conductor. This effect can be exploited and the two EDUs can be complementary to each other when maximizing the overall power-train efficiency under different vehicle operating conditions.

Since the electric motors used in the front and rear EDU are both PMSMs, the EDUs are subject to high no-load losses when the electric motors are under free-spinning (no-load) conditions, especially at higher speeds, as shown in Fig. 5. The no-load losses consist of two parts, namely i) losses generated by the inverter and PMSM when supplying reactive current to reduce the back EMF induced by the permanent magnets and ii) losses generated by mechanical friction components inside the EDU.

2.3. Battery system

Both front and rear EDU are supplied by the same lithium-ion battery pack which is modeled by an equivalent circuit [35–37] with an open circuit voltage, V_{oc}, and an internal battery resistance, R_i. The battery state of charge (SoC) can be calculated as

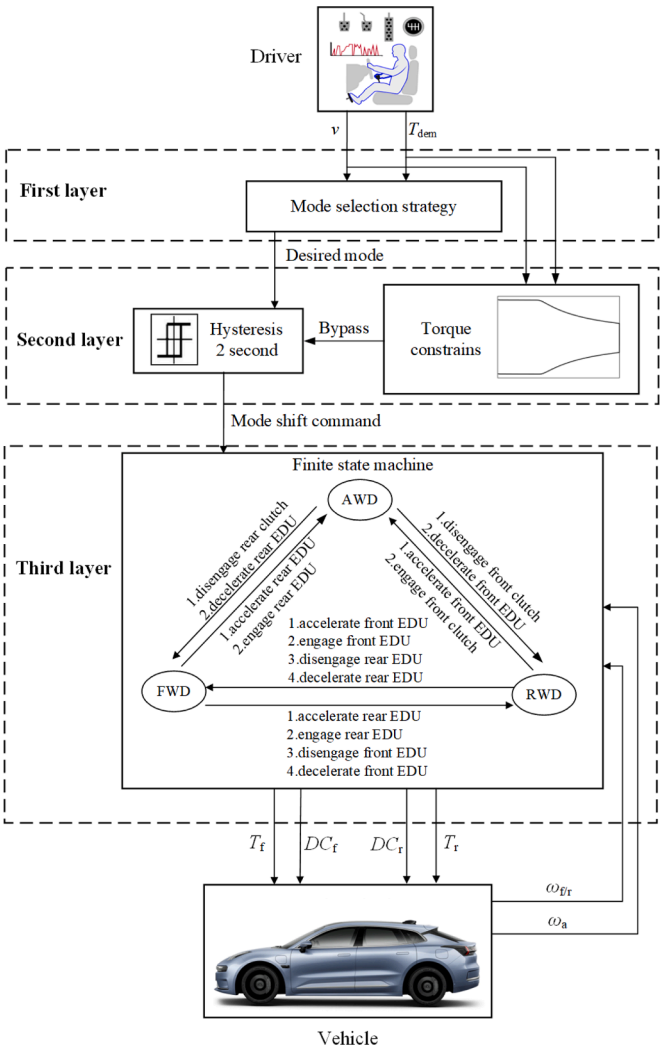

Fig. 7. Structure of powertrain hierarchical controller.

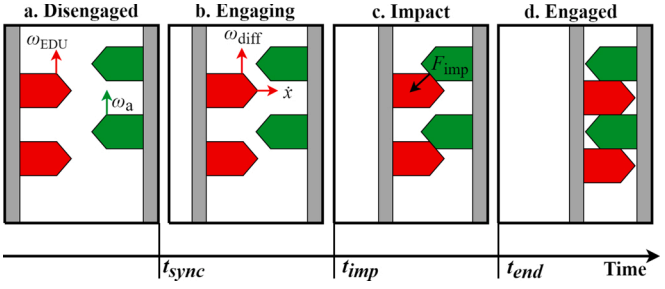

Fig. 8. Dog clutch engagement processes.

$$\mathrm{SoC}(t) = \mathrm{SoC}(t_0) + \int_{t_0}^{t} -\frac{1}{C_b} \frac{V_{oc} - \sqrt{V_{oc}^2 - 4R_i P_b(t)}}{2R_i} \, \mathrm{dt} \tag{2}$$

where $\mathrm{SoC}(t_0)$ is the initial battery SoC, C_b is the battery capacity, and P_b is the terminal output power of the battery. Typically, the open circuit voltage, V_{oc}, and internal resistance, R_i, vary with the SoC and charging/discharging state.

2.4. Dog clutch

To connect and disconnect the EDU with the drive axle, the EDU output shaft and drive axle are coupled by a dog clutch. The dog clutch is actuated by a DC shifter motor through a fork, as illustrated in Fig. 6. From supplier measurement data, it is determined that each clutch engagement or disengagement takes about 300ms corresponding to an average energy consumption of 16 kJ. When the clutch is engaged, a power consumption of 5Wh is continuously drawn.

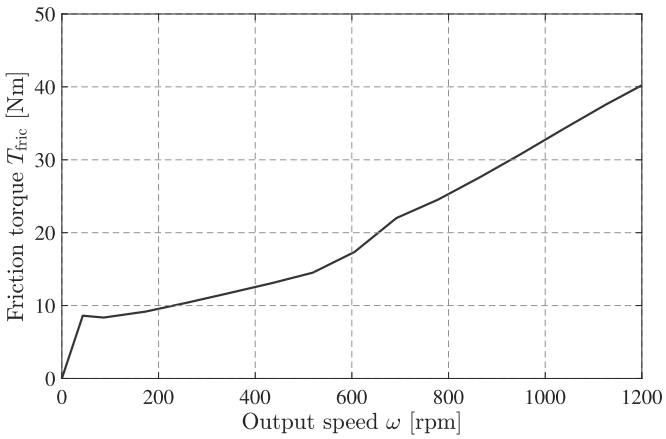

Fig. 9. EDU friction torque.

2.5. Hierarchical powertrain controller

A hierarchical powertrain controller, as depicted in Fig. 7, is proposed in order to utilize the flexibility of the powertrain operating modes for maximizing the energy efficiency of the powertrain. As shown, the whole control process is divided into three layers.

In the first layer, according to the operating mode selection strategy (discussed in Section 4), the desired operating mode is preliminarily selected to maximize the powertrain efficiency based on the vehicle speed, v, and the vehicle torque demand, T_{dem}. The second layer introduces a hysteresis delay time of 2s to prevent frequent mode shifts and clutch toggling. However, in case of a high, instantaneous torque demand step, which can be only handled by AWD mode, the hysteresis delay will be bypassed and AWD mode will be adopted immediately. In the third layer, based on the mode shift command perceived from the upper layers, a finite state machine coordinates the clutch actuation signals and the torque demand to the EDUs. During mode shift transitions, the corresponding EDU speed is controlled to cope with the clutch engagement and disengagement process, which will be discussed in the following section. Based on the drive axle (ω_a) and EDU speed (ω_f and ω_r), which are obtained from vehicle sensors, the clutch engagement or disengagement execution command, DC, is sent to the corresponding clutch. To distinguish between the engagement or disengagement execution command for the front and rear clutch, these are respectively denoted as DC_f and DC_r.

3. EDU speed control during mode shift transitions

3.1. Background

The engagement process of a dog clutch involves four stages, as illustrated in Fig. 8. Before the dog clutch starts to engage in the first stage, it is necessary to synchronize the rotational speed of the EDU output shaft and drive axle ω_a. To distinguish between the front and rear EDU speeds, these are respectively denoted as ω_f and ω_r. The shifter motor starts to actuate the fork for the engaging process only when the speed difference, $|\omega_{diff}|$, between both shafts is within a certain range to ensure a successful engagement and less clutch wearing (12 rpm for the clutch used in this study) [38,39].

During mode shift transitions, the EDU controller enters speed con-

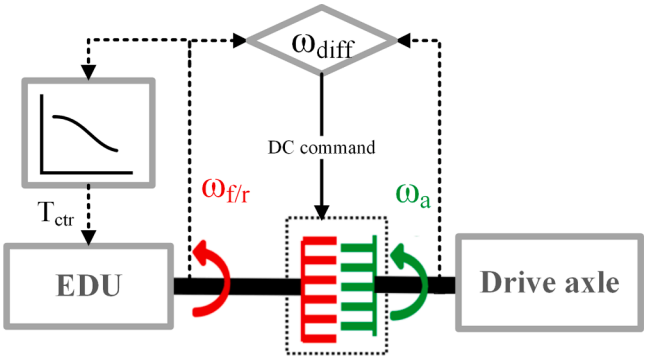

Fig. 11. The scheme of energy-efficient EDU speed control process.

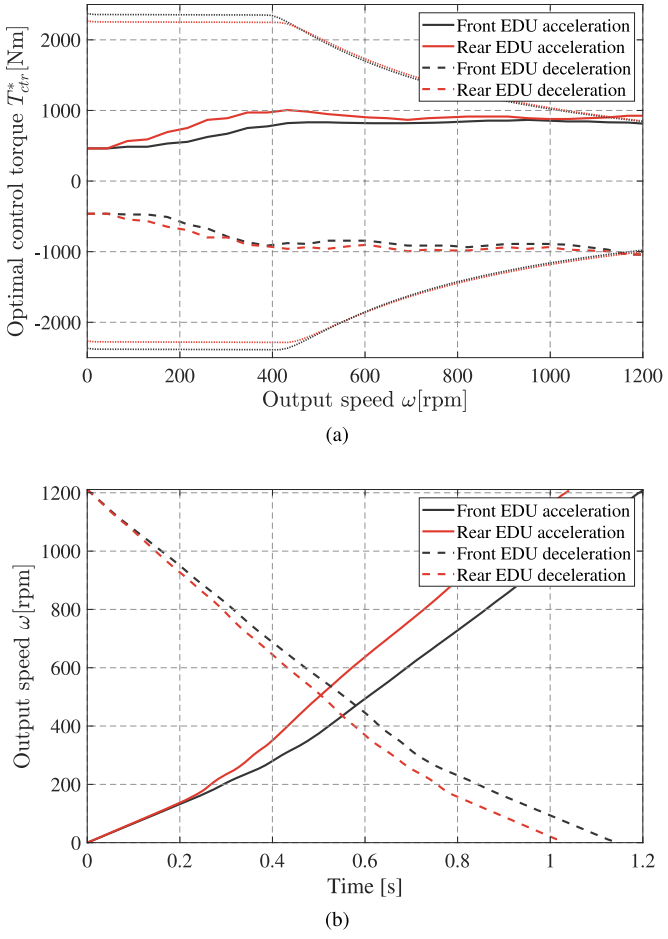

Fig. 10. Energy-efficient EDU speed control (a) torque trajectories and (b) corresponding EDU speed response.

trol mode where the EDU speed is accelerated and synchronized to match the rotational speed of the drive axle. On the other hand, once the EDU is disconnected from the drive axle, the EDU speed should be decelerated down to zero to not only recover the rotating kinetic energy but also to get rid of the no-load losses. The EDU speed is controlled by sending a speed control torque (T_{ctr}) request to the EDU, to overcome the moment of inertia and friction torque,T_{fric}, until the EDU reaches the desired speed according to

$$T_{\text{ctr}} = J\frac{\mathrm{d}\omega}{\mathrm{dt}} + T_{\text{fric}} \tag{3}$$

where J and ω are the inertia of the rotational parts and the rotational

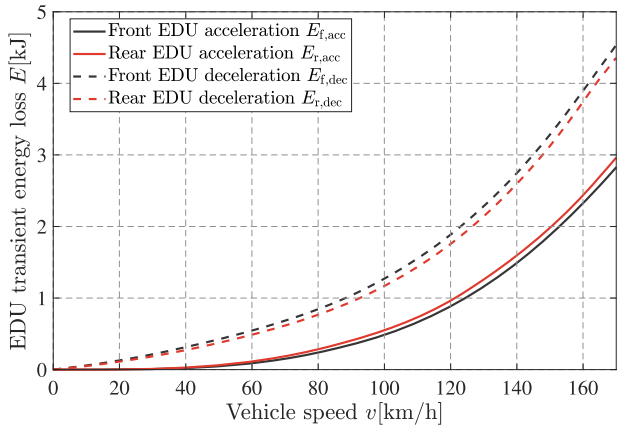

Fig. 12. EDU transient energy loss during the speed control process.

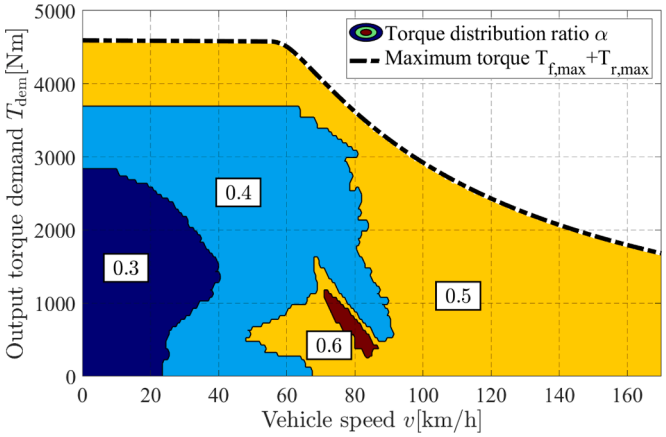

Fig. 13. Optimal torque distribution ratio α_{opt} in AWD mode.

speed of the EDU output shaft, respectively. The friction torque of both EDUs shown in Fig. 9 is the same since the friction torque of the whole EDU rotating part is not affected by PMSM's winding topology.

To cope with the speed dynamics and to ensure fast speed control, a high torque demand, up to the maximum and minimum output torque of the EDU, is normally used. However, the speed control process causes energy losses during each mode shift transition. From an energy efficiency point of view, fast EDU speed control induces higher loss since the EDU efficiency is very low when operating at the maximum or minimum torque boundary. Usually, as assumed in this study, the mode shift transition response is not a time-critical factor. Therefore, an energy-efficient EDU speed control to minimize this part of the energy losses is proposed in the following subsection.

3.2. Energy-efficient EDU speed control

The energy-efficient EDU speed control torque is defined as a torque trajectory in reference to the EDU speed, meaning that the optimal (energy-efficient) control torque relative to EDU speed can be simply precalculated and stored in a lookup table. As shown in Fig. 11, based on the monitored current EDU speed, the speed control torque is updated to the optimal (energy-efficient) control torque value from the lookup table and in turn sent back to EDU. The energy-efficient EDU speed control torque is derived as follows.

Firstly, the EDU speed control process from an initial speed, ω_0, to a desired speed, ω_N, is divided into a series of N sub-processes ($[\omega_0, \omega_1]$, $[\omega_1, \omega_2]$ ... $[\omega_{N-1}, \omega_N]$). For simplicity, the EDU speed control torque is assumed to be constant during each sub-process. For a given EDU speed control torque value, T_{ctr}, the energy losses induced during each sub-

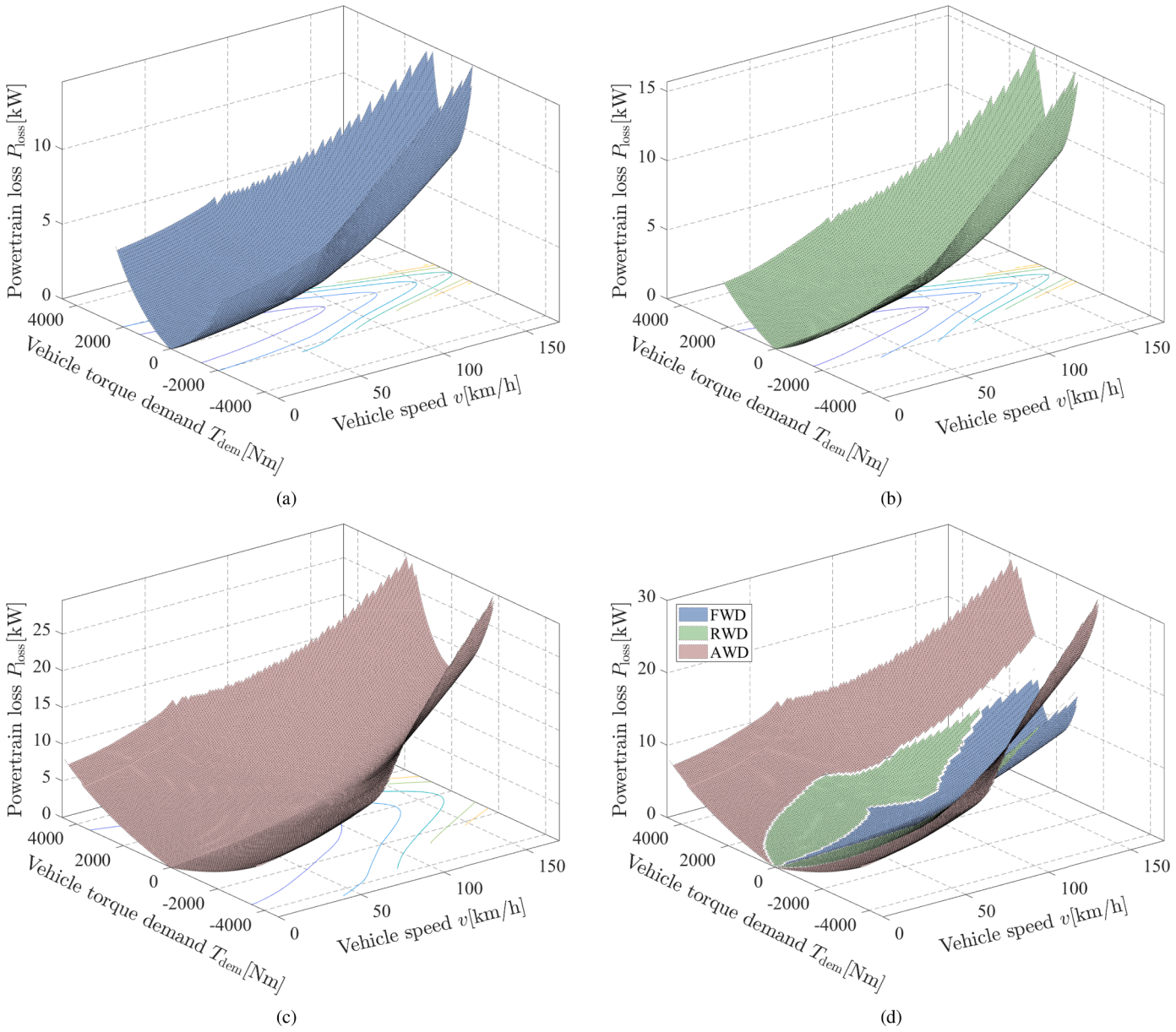

Fig. 14. Powertrain loss in (a) FWD, (b) RWD (c) AWD mode and (d) the minimum powertrain loss.

process can be calculated by iterating the calculation over a series of time steps. During each iteration, the EDU speed for a given speed control torque changes according to

$$\omega_{i+1} = \frac{\left(T_{\text{ctr}} - T_{\text{fric}}(\omega_i)\right)\Delta t}{J} \tag{4}$$

where Δt is the time step size and ω_i is the rotational speed of the EDU output shaft at each time step i.

Besides, the energy losses of the EDU during each sub-process can be calculated as

$$E_{\text{ctr}} = \sum_{i=1}^{N} P_{\text{loss},i}(\omega_i, T_{\text{ctr}})\Delta t \tag{5}$$

where $P_{\text{loss,i}}$ corresponds to the EDU power losses at the ith time step. Based on the EDU efficiency, the energy-efficient EDU control torque, T^*_{ctr}, resulting in the minimal energy losses for each sub-process, can be derived. By repeating this procedure for the entire speed control range, the energy-efficient EDU speed control torque values of the front and rear EDU during speed control are derived. For instance, the energy-efficient torque trajectories and corresponding EDU speed response are illustrated in Fig. 10.

Given the derived energy-efficient EDU speed control torque trajectories, the transient energy losses during acceleration from 0 to a target speed and deceleration from a certain speed to 0 can be estimated and stored as a look-up table relative to the target speed and operating speed as shown in Fig. 12. For convenience, it is mapped in reference to the vehicle speed at which the mode shift and EDU speed control process starts (for example, the vehicle speed to which the EDU must be accelerated and synchronized and the vehicle speed from which EDU is disconnected and decelerated), given the relationship between the vehicle speed and EDU speed as:

$$v = \frac{1000 \cdot R_r \cdot \omega \cdot 2\pi}{3600 \cdot 60} \tag{6}$$

4. Operating mode selection strategy

The complementary efficiency difference between the front and rear

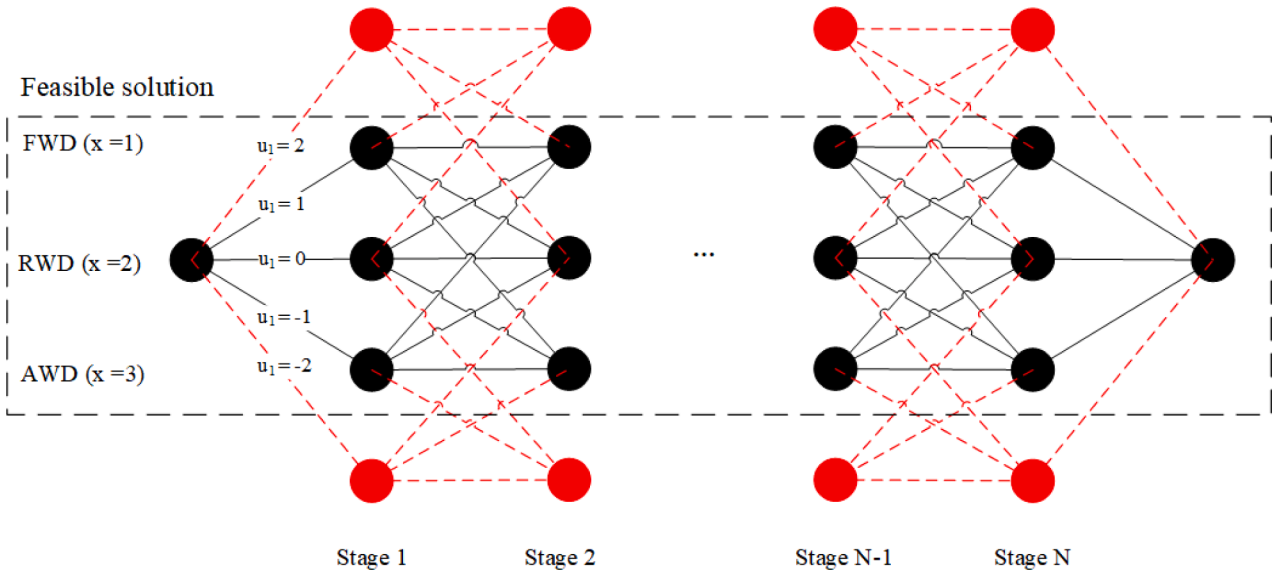

Fig. 15. Illustration of DP optimization process.

EDU results in different powertrain losses (consisting of front and rear EDU losses) for each operating mode. Thus, the powertrain energy efficiency can be maximized by the proper selection of the operating mode. Besides, the AWD mode offers an additional degree of freedom to minimize the powertrain losses by the optimal distribution of the torque between the front and rear EDU. The details of deriving the optimal torque distribution strategy in AWD mode and determining the most energy-efficient operating mode are given in the following subsections.

4.1. Optimal torque distribution strategy in AWD mode

When the powertrain is operating in AWD mode, the vehicle torque demand for propelling or braking the vehicle can be distributed to the front and rear EDU as follows

$$T_{\mathrm{dem}} = T_{\mathrm{f}} + T_{\mathrm{r}} \tag{7}$$

where T_{f} and T_{r} are the torque provided by the front and rear EDU.

To better formulate the optimization problem of the torque distribution, a torque distribution ratio, α, is introduced so that T_{f} and T_{r} can be substituted as:

$$\begin{cases} T_{\mathrm{f}} = \alpha T_{\mathrm{dem}} \\ T_{\mathrm{r}} = (1-\alpha) T_{\mathrm{dem}} \end{cases} \tag{8}$$

The power losses of the EDUs depend on the combination of their operating speed and torque, which means an optimal distribution ratio, α, can be found to minimize the overall losses of both EDUs (when given a certain combination of vehicle speed and driver torque demand). The torque distribution optimization problem can therefore be formalized as follows:

$$J = \min\left\{P_{\mathrm{loss,f}}\left(\omega_{\mathrm{f}}, \alpha T_{\mathrm{dem}}\right) + P_{\mathrm{loss,r}}\left(\omega_{\mathrm{r}}, \alpha T_{\mathrm{dem}}\right)\right\} \tag{9}$$

with the constraints of

$$\begin{cases} T_{\mathrm{f,min}}\left(\omega_{\mathrm{f}}\right) \le \alpha T_{\mathrm{dem}} \le T_{\mathrm{f,max}}\left(\omega_{\mathrm{f}}\right) \\ T_{\mathrm{r,min}}\left(\omega_{\mathrm{r}}\right) \le (1-\alpha) T_{\mathrm{dem}} \le T_{\mathrm{r,max}}\left(\omega_{\mathrm{r}}\right) \\ \alpha \in [0,1] \end{cases} \tag{10}$$

where $P_{\mathrm{loss,f}}$ are the front EDU losses, $P_{\mathrm{loss,r}}$ are the rear EDU losses, $T_{\mathrm{f,min}}$ is the minimum torque of the front EDU, $T_{\mathrm{f,max}}$ is the maximum torque of the front EDU, $T_{\mathrm{r,min}}$ is the minimum torque of the rear EDU and $T_{\mathrm{r,max}}$ is the maximum torque of the rear EDU.

For convenience, the vehicle speed is used as the reference speed. For each combination of vehicle speed and vehicle torque demand, the optimal torque distribution ratio, α_{opt}, can be derived based on the loss information of the EDUs using an offline grid search method [40,41]. The optimal torque distribution ratio is shown in Fig. 13. It is worth noting that the optimal torque distribution strategy derived in AWD mode also represents the optimal operating strategy of the FRID powertrain. As shown, when two EDUs with different efficiency characteristics are deployed, the optimal torque distribution ratio is not always 0.5, which is valid for two identical EDUs [25]. Furthermore, considering the no-load losses of the EDUs, it is more efficient to use both front and rear EDU together even under low torque operating conditions.

4.2. Rule-based operating mode selection strategy

To identify the mode selection strategy to choose the most energy-efficient operating mode under different vehicle driving conditions, the powertrain losses in each operating mode are mapped in reference to the vehicle speed and torque demand according to (9). For AWD mode, an optimal torque distribution strategy with α_{opt} is taken into account. For FWD and RWD modes, the torque split ratio, α, is substituted by 1 and 0, respectively. Consequently, by comparing the powertrain losses for different operating modes, the rule-based mode selection strategy which selects the most energy-efficient mode with minimum powertrain loss can be obtained. The mapped powertrain losses for different operating modes, together with the minimum powertrain losses, are shown in Fig. 14.

4.3. Predictive mode selection strategy

To fully realize the energy-saving potential of AFRID powertrains, the energy losses induced by mode shifts need to be taken into account. In this section, a predictive mode selection strategy is proposed. With vehicle route information beforehand, the speed profile is treated as known information. Hence, the mode selection can be optimized with the help of global optimization tools. As a powerful optimization tool, dynamic programming (DP) algorithms have been extensively used to find the optimal control strategy for energy management systems in electrified vehicle applications over the recent years [42–44]. The DP algorithm deals with situations where decisions are made at each stage,

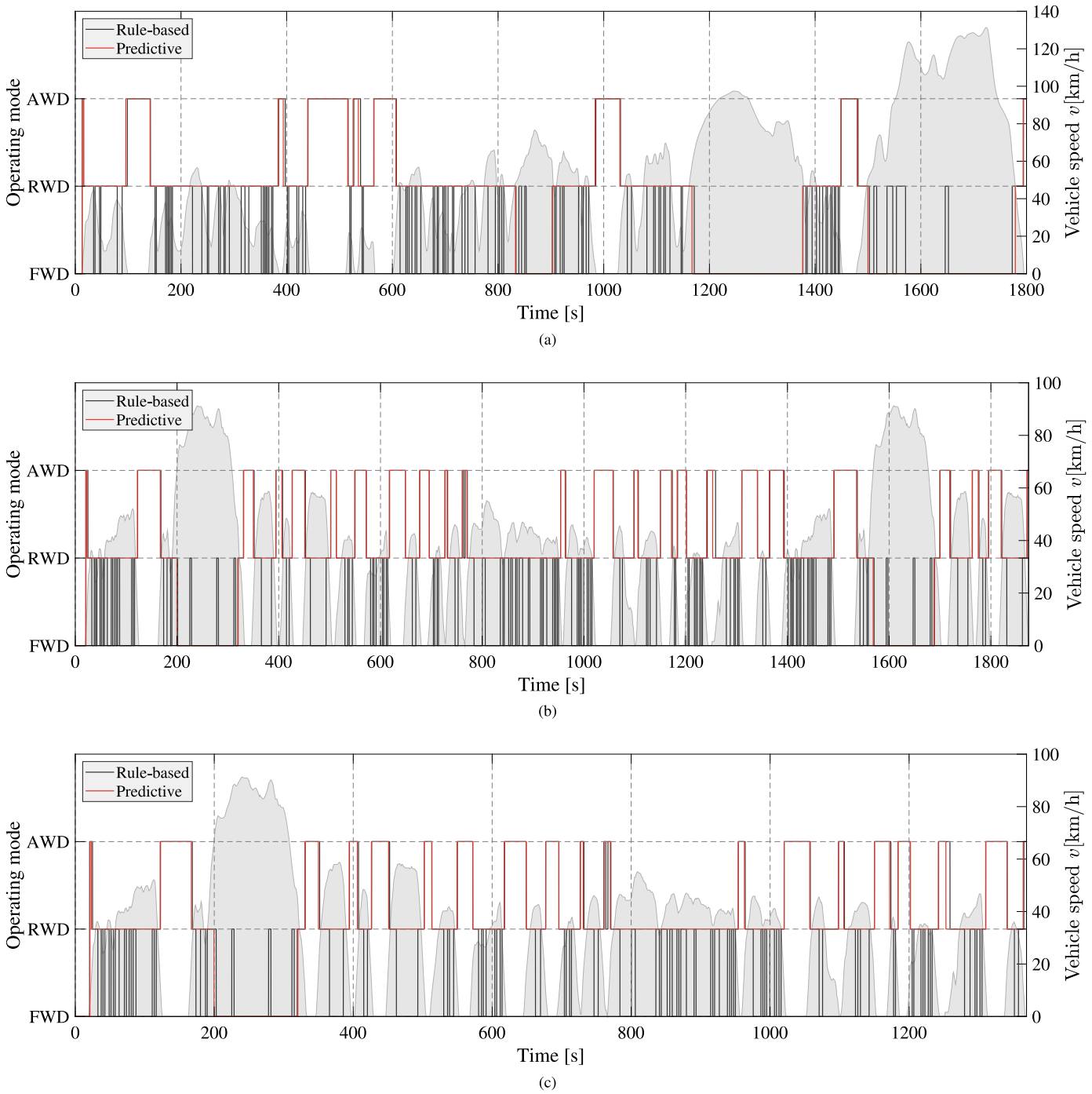

Fig. 16. Comparison of operating mode with rule-based and predictive mode selection strategy under (a) WLTC, (b) FTP75 and (c) UDDS cycles.

with the objective to minimize or maximize a certain cost function and obtain a globally optimal solution.

4.3.1. Problem formulation

For the investigated AFRID powertrain, the optimization problem is to find an optimal operating mode sequence that minimizes the overall powertrain losses with the consideration of the induced energy losses during mode shift transitions. The powertrain operating mode is chosen as the only state variable x with three possible integer values: 1, 2, and 3 which represent the FWD, RWD, and AWD modes, respectively. Consequently, the control variable, operating mode shift command, u, which is an integer within the range $[-2, 2]$, represents different mode shift commands. The description of the DP optimization process is illustrated in Fig. 15. The investigated driving cycle is discretized into N stages in the horizontal direction. The time response of the EDU speed control during mode shift transition is mostly within one second except in extreme cases where the EDU speed needs to be accelerated or decelerated between 0 and maximum EDU speed. Thus, one second is an appropriate time step ΔT for each stage. At each stage k, the vehicle speed v_k is a known input from the driving cycle. Hence, the driver torque demand $T_{\text{dem},k}$ can be derived by the discretized form of (1). The powertrain loss at each stage, $P_{\text{loss},k}(x, v_k, T_{\text{dem},k})$, is dependent on the powertrain operating mode, x_k, and calculated according to the powertrain loss maps as derived in the previous section. The powertrain operating mode, x_k, together with the operating mode shift command, x_k, determine the new operating mode, $x_{k+1} = x_k + u_k$, in the next stage.

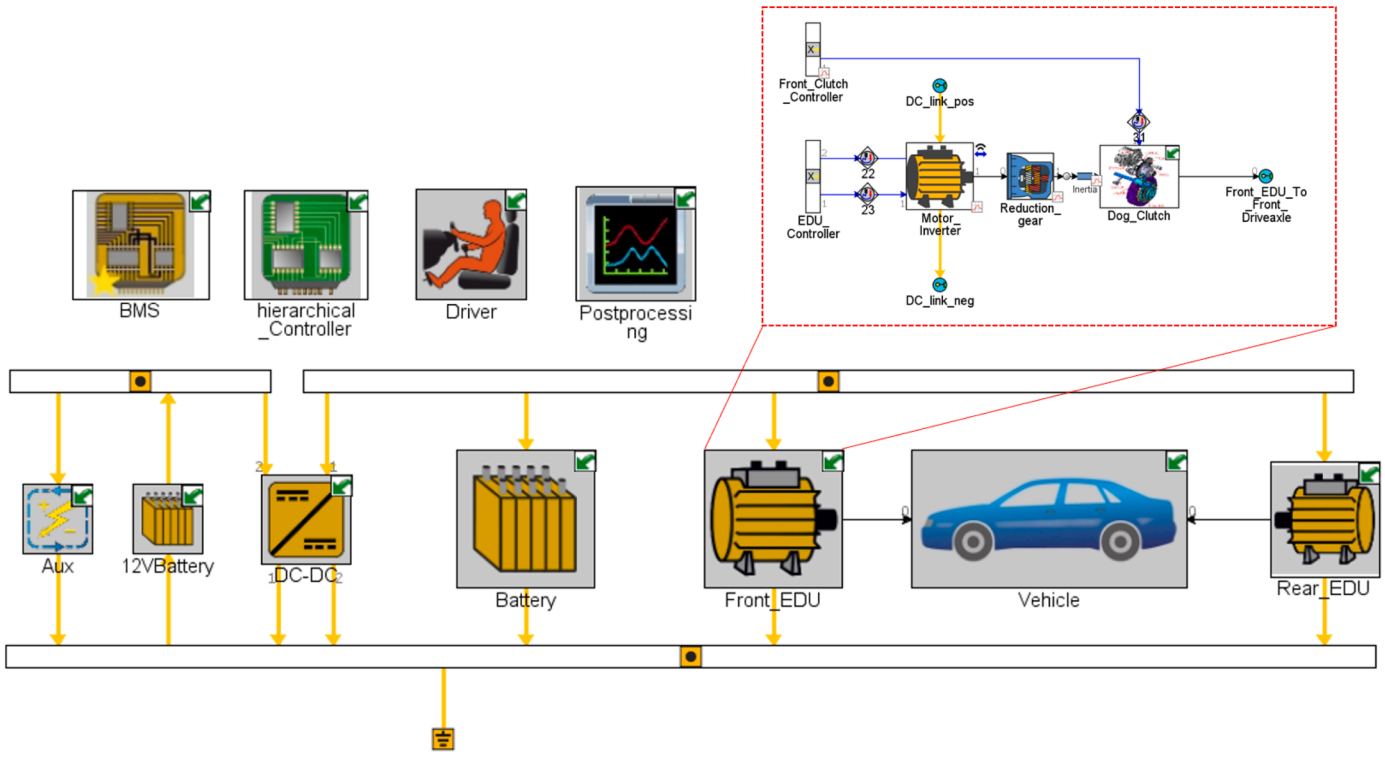

Fig. 17. GT-suite powertrain model architecture.

Table 3
Simulation results under WLTC, FTP75 and UDDS driving cycles.

Cycle	Powertrain	Mode selection strategy	Energy cons. [kWh/100km]	Improvement	Number of mode shifts
WLTC	FRID	-	22.17	-	-
	AFRID	Rule-based	20.50	7.53%	143
	AFRID	Predictive	20.35	8.21%	23
	Single motor *	-	20.46	7.71%	-
FTP75	FRID	-	17.08	-	-
	AFRID	Rule-based	15.94	6.67%	199
	AFRID	Predictive	15.73	7.90%	51
	Single motor	-	16.00	6.32%	-
UDDS	FRID	-	16.39	-	-
	AFRID	Rule-based	15.33	6.47%	153
	AFRID	Predictive	15.11	7.81%	39
	Single motor	-	15.40	6.04%	-

*EDU with stranded winding PMSM is used for single motor powertrain simulation.

Infeasible modes ($x_k \neq 1,2,3$) are excluded.

The objective function of the DP consists of two terms, powertrain energy losses due to vehicle propulsion and regeneration, and energy losses caused by mode shift transitions. Therefore, the objective function can be formulated as follows:

$$J = \min \sum_{k=0}^{N-1} \Delta T \cdot P_{\text{loss},k}\left(x, v_k, T_{\text{dem},k}\right) + E_{\text{shift},k}\left(x_k, u_k\right) \tag{11}$$

with the constraints of

$$\begin{cases} 1 \leq x_k \leq 3 \\ T_{\min}(x_k, v_k) \leq T_{\text{dem},k} \leq T_{\max}(x_k, v_k) \end{cases} \tag{12}$$

where ΔT is the time step of each stage, $P_{\text{loss},k}(x, v_k, T_{\text{dem},k})$ is the powertrain loss at stage k and $E_{\text{shift},k}(x_k, u_k)$ is the EDU transient energy loss for a given mode shift command, u_k, and mode state, x_k. $T_{\min}(x_k, v_k)$ and $T_{\max}(x_k, v_k)$ are the minimum and maximum torque capability of operating mode x_k.

With different operating mode shifts, the transient energy loss, $E_{\text{shift},k}(u_k)$, associated with mode shifts is calculated as

$$\begin{cases} E_{1,2} = E_{\text{r,acc}}(v) + E_{\text{f,dec}}(v) \\ E_{2,1} = E_{\text{f,acc}}(v) + E_{\text{r,dec}}(v) \\ E_{1,3} = E_{\text{r,acc}}(v) \\ E_{3,1} = E_{\text{r,dec}}(v) \\ E_{2,3} = E_{\text{f,acc}}(v) \\ E_{3,2} = E_{\text{f,dec}}(v) \end{cases} \tag{13}$$

where $E_{\text{i,j}}$ is the transient mode shift energy loss when shifting the powertrain operating mode from mode i to j, $E_{\text{f/r,acc}}(v)$ is the front or rear EDU energy loss caused by accelerating the EDU speed to match the vehicle speed, v, and $E_{\text{f/r,dec}}(v)$ is the front/rear EDU energy loss caused by decelerating the EDU speed to zero. Both $E_{\text{f/r,acc}}(v)$ and $E_{\text{f/r,dec}}(v)$ are derived in Fig. 12.

4.3.2. Optimized mode selection

The optimal operating modes derived from DP optimization for the WLTC, FTP-75 and UDDS driving cycles are shown in Fig. 16 and compared to the ones derived by the rule-based mode selection strategy. Fewer operating mode shifts and more portions of AWD mode are seen for the DP-optimized mode selection with future route information. Right before each vehicle stop, AWD mode is selected during the deceleration and utilized for the next vehicle starting acceleration. This is as expected since AWD mode is more efficient for vehicle stop and start phases where high torque is demanded at low speed. In the meanwhile, the transient energy loss caused by shifting to AWD mode is much lower at these low-speed phases.

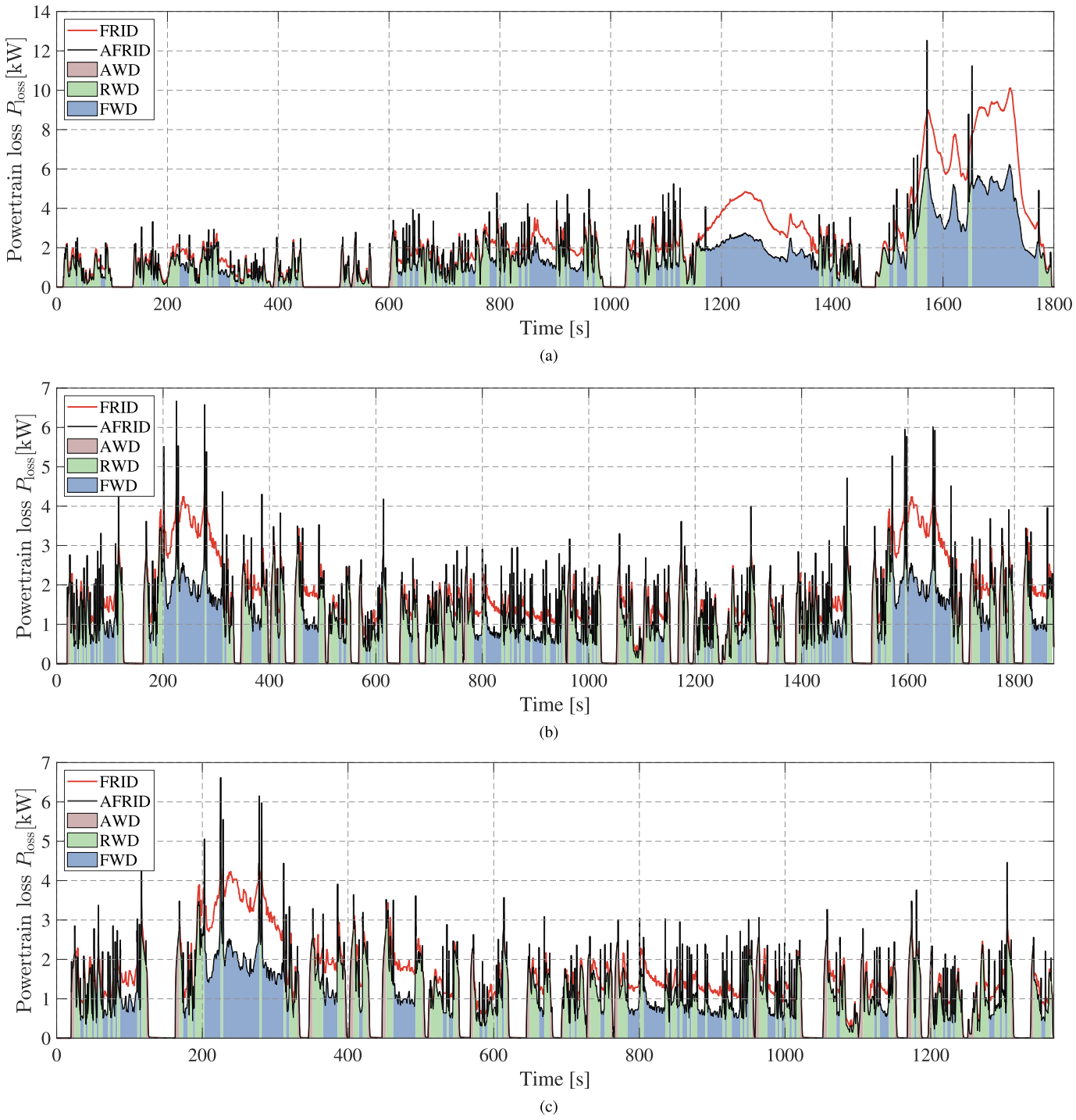

Fig. 18. Comparison of powertrain loss between FRID powertrain and AFRID powertrain with rule-based mode selection strategy under (a) WLTC, (b) FTP75 and (c) UDDS driving cycles.

5. Simulation results and discussion

In this section, the energy consumption improvement of the AFRID powertrain is verified in comparison to the conventional FRID powertrain using simulations. It is worth noting that the conventional FRID powertrain only operates in AWD mode with the optimal torque distribution strategy. The simulations are carried out in GT-Suite where the complete powertrain system model, together with the hierarchical powertrain controller, is built and implemented as schematically illustrated in Fig. 17. To evaluate the energy efficiency improvement by the AFRID powertrain under different driving conditions, three standard test driving cycles are investigated, WLTC, FTP75 and UDDS.

The simulation results are summarized in Table 3. Compared to the FRID powertrain, the AFRID powertrain achieves a significant energy consumption reduction for all three driving cycles. The comparison of the powertrain losses between the FRID powertrain and AFRID powertrain with the derived rule-based mode selection strategy is illustrated in Fig. 18. It can be observed that the AFRID powertrain mostly operates in FWD or RWD mode with only one EDU activated unless the torque demand is high, as for instance during a fast acceleration event such as the vehicle start-up phase. This aspect allows the AFRID powertrain to achieve lower powertrain losses in general.

Table 4
Comparison of solution with other FRIDs [45].

Vehicle model	Powertrain	Vehicle mass [kg]	WLTC cons. [kWh/100km]	Improvement
Polestar 2 Long range	Dual PMSMs FRID	2113	17.0	-
	Single PMSM	1994	19.4	-12.4%
Tesla Model Y	IM / PMSM FRID	1995	17.0	-
	Single PMSM	1909	15.5	-8.8%
Volvo C40 Recharge	Dual PMSMs FRID	2185	20.7	-
	Single PMSM	2021	18.2	-12.1%

In addition, the energy consumption of the FRID powertrain is 7.71%, 6.32% and 6.04% higher in comparison to the single motor powertrain for the WLTC, FTP75 and UDDS driving cycles, respectively. These results show the trend in accordance to Grunditz and Thiringer [23] and publicly available data from existing EVs on the market, such as shown in Table 4. Since the dual motor system of the Tesla model Y comprises one induction machine, the WLTC energy consumption in relation to the single motor variant shows a better trend than that of the Volvo C40 recharge or the Polestar 2. It should be noted that the vehicles in Table 4 have a lower curb weight and hence a reduced energy consumption compared to the investigated vehicle in this paper. Nonetheless, despite the torque distribution capability of the PMSM-based FRID powertrain, the energy efficiency decreases compared to the single motor powertrain. However, with the help of the clutches and disconnect functionality of the AFRID powertrain, the decreased energy efficiency of the dual motor solution can be almost fully mitigated while maintaining the advantages of FRID powertrains.

5.1. Impact of energy losses during mode shift transitions

It should be noted that many powertrain loss-spikes are observed in the AFRID powertrain with the rule-based mode selection strategy during mode transitions. Driving conditions can vary greatly during driving cycles, leading to frequent mode shifts and a high number of EDU connection and disconnection events triggered by the rule-based strategy. As a result, the energy losses during these transitions accumulate to a substantial amount.

To evaluate the effect of energy losses during mode shift transitions on the total energy consumption, a baseline scenario is studied where the EDU speed is accelerated and decelerated using maximum and minimum torque rather than energy-efficient EDU speed control torque. The obtained, comparative results are shown in Table 5. Under the three driving cycles, significant amounts of the overall powertrain losses are due to EDU energy losses dissipated during operating mode transitions (3.46% to 7.30%). The amount of energy loss can be reduced by applying an energy-efficient EDU speed control, which leads to a reduction in the overall vehicle energy consumption by 0.63%, 1.36% and 1.54% for the three driving cycles. Since the FTP75 and UDDS driving cycles involve more dynamic operating conditions and mode shifts compared to the WLTC, minimizing the energy loss during mode

Table 5
Comparison of max/min torque and energy-efficient EDU speed control for the WLTC, FTP75 and UDDS driving cycles.

Cycle	EDU speed control	Energy cons. [kWh/100km]	Improvement	Transition loss [kWh/100km]	Overall powertrain loss [kWh/100km]	Transition /Overall
WLTC	Max/min torque	20.63	-	0.13	3.19	4.08%
	Energy-efficient	20.50	0.63%	0.10	3.14	3.46%
FTP75	Max/min torque	16.16	-	0.21	3.12	6.73%
	Energy-efficient	15.94	1.36%	0.16	3.10	5.16%
UDDS	Max/min torque	15.57	-	0.23	3.15	7.30%
	Energy-efficient	15.33	1.54%	0.17	3.13	5.43%

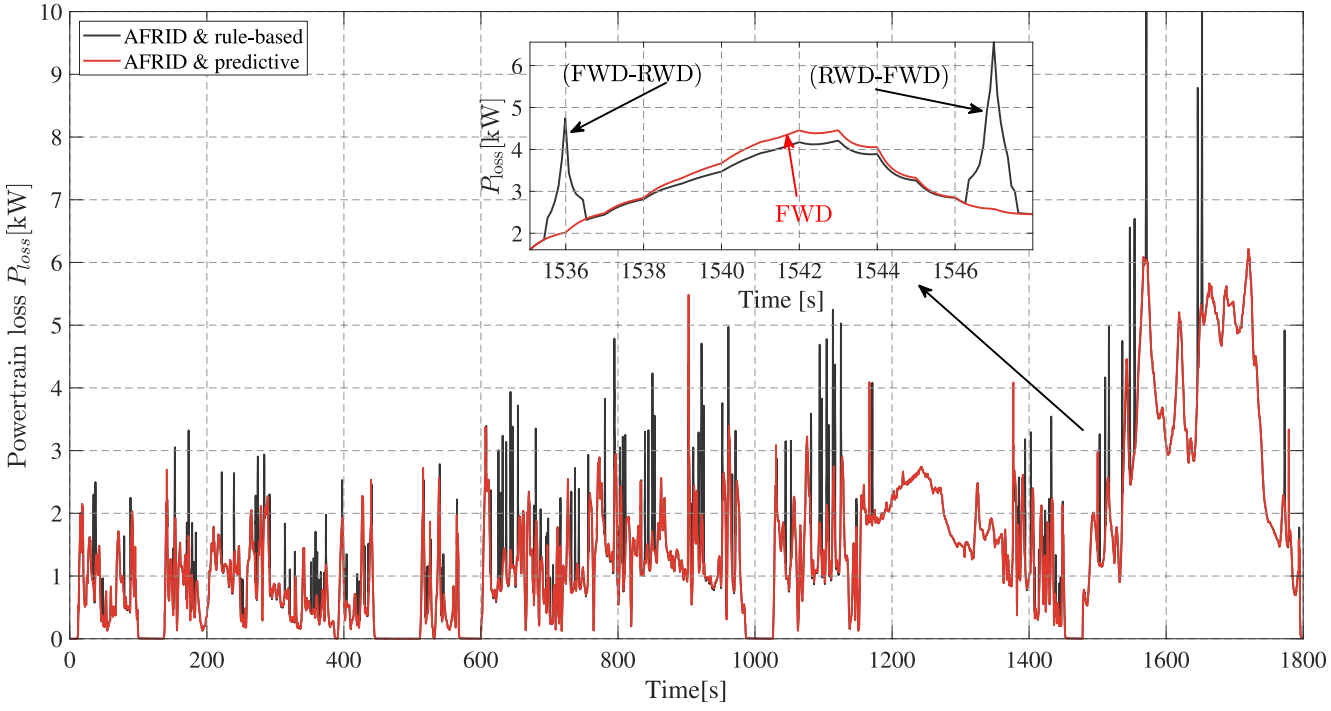

Fig. 19. Powertrain loss of AFRID with predictive and rule-based mode selection strategy during the WLTC.

shift transitions results in a greater reduction in energy consumption.

5.2. Advantages of the predictive operating mode selection strategy

The results in Table 3 also point out that with the predictive mode selection strategy, the number of mode shifts is significantly reduced by 83.92%, 74.37% and 74.51% for WLTC, FTP75 and UDDS driving cycles, respectively. The decrease in the number of shifts in operating mode reduces the strain on the clutch and related actuation mechanisms, prolonging their lifespan. At the same time, fewer shifts also result in decreased energy consumption. On top of the benefit of disconnect functionality in the AFRID powertrain, additional 0.68%, 1.23% and 1.34% energy consumption reduction can be achieved for the three driving cycles. This is due to the fact that while the rule-based mode selection strategy enables the powertrain to transition to the most energy-efficient mode at each moment, not all transitions result in energy savings in the powertrain as the energy losses caused by transitions themselves can be detrimental. To demonstrate such phenomenon in a more detailed way, the AFRID powertrain losses with rule-based and predictive mode selection strategy during the WLTC are shown in Fig. 19. During the time interval between 1536s and 1548s, the rule-based mode selection strategy executes mode shifts from FWD mode to RWD mode and later back to FWD mode. However, the predictive mode selection strategy chooses to stay in FWD mode during the time interval. As can be seen from the figure, even though RWD mode leads to reduced powertrain losses compared to the FWD mode during this period, the reduced energy loss over the time interval is still significantly less than the additional transient loss caused by mode shifts. In this scenario, the use of a rule-based mode selection strategy results in lower energy efficiency due to the increase in mode shifts. However, with the predictive mode selection strategy, excessive mode shifts can be prevented using pre-known route information. This is especially relevant in public transportation, where similar routes are repeated daily, and in autonomous vehicles that use live mapping systems. The predictive mode selection strategy further reduces the energy consumption of the AFRID powertrain by balancing the advantages of operating the powertrain in the most energy-efficient mode with the transient losses caused by the corresponding shift.

6. Conclusion

This study investigated the potential for improving the energy efficiency of an AFRID powertrain with disconnect functionality. The utilization of a clutch between the EDU and the drive axle reduces the no-load losses of the PMSMs. The study proposed a rule-based powertrain operating mode selection strategy that considers front-rear torque distribution. The energy-saving potential of the AFRID powertrain was evaluated for the WLTC, FTP75 and UDDS. The simulation results showed that the AFRID powertrain and rule-based mode selection strategy reduced the energy consumption by 7.53%, 6.67% and 6.47% for the WLTC, FTP75 and UDDS driving cycles, respectively, compared to a FRID powertrain.

The study also assessed the impact of energy losses during mode shift transitions on the overall energy consumption. The proposed energy-efficient EDU speed control process for the AFRID powertrain during mode shifts further reduced the energy consumption by 0.63%, 1.36% and 1.54% for the WLTC, FTP75 and UDDS respectively.

Finally, the study investigated a predictive mode selection strategy that uses DP-based optimization and predictive route information to avoid excessive mode shifts. This approach achieved an additional 0.68%, 1.23%, and 1.34% reduction in energy consumption for the WLTC, FTP75 and UDDS, as well as a significant decrease in clutch actuations.

CRediT authorship contribution statement

Y. Xu: Conceptualization, Methodology, Formal analysis, Software, Writing – original draft. **A. Kersten:** Conceptualization, Formal analysis, Writing – review & editing, Visualization. **S. Klacar:** Conceptualization, Writing – review & editing, Supervision. **B. Ban:** Writing – review & editing, Visualization. **J. Hellsing:** Writing – review & editing, Project administration. **D. Sedarsky:** Writing – review & editing, Supervision.

Declaration of Competing Interest

The authors declare that they have no known competing financial interests or personal relationships that could have appeared to influence the work reported in this paper.

Data availability

Data will be made available on request.

Acknowledgment

This work was supported by the Swedish Energy Agency program for vehicle research and innovation (FFI), grant number 51459-1.

References

[1] J. Buberger, A. Kersten, M. Kuder, R. Eckerle, T. Weyh, T. Thiringer, Total CO2-equivalent life-cycle emissions from commercially available passenger cars, Renew. Sustain. Energy Rev. 159 (2022) 112158.
[2] M.S. Kumar, S.T. Revankar, Development scheme and key technology of an electric vehicle: an overview, Renew. Sustain. Energy Rev. 70 (2017) 1266–1285.
[3] V. Etacheri, R. Marom, R. Elazari, G. Salitra, D. Aurbach, Challenges in the development of advanced li-ion batteries: a review, Energy Environ. Sci. 4 (9) (2011) 3243–3262.
[4] C.C. Chan, The state of the art of electric, hybrid, and fuel cell vehicles, Proc. IEEE 95 (4) (2007) 704–718.
[5] E. Helmers, P. Marx, Electric cars: technical characteristics and environmental impacts, Environ. Sci. Eur. 24 (1) (2012) 1–15.
[6] M.A. Roscher, R. Michel, W. Leidholdt, Improving energy conversion efficiency by means of power splitting in dual drive train EV applications, Int. J. Veh. Technol. 2013 (2013).
[7] W. Da, W. Bo, Research on driving force optimal distribution and fuzzy decision control system for a dual-motor electric vehicle. 2015 34th Chinese Control Conference (CCC), IEEE, 2015, pp. 8146–8153.
[8] N. Mutoh, Front-and-rear-wheel-independent-drive-type electric vehicle (FRID EV) with compatible driving performance and safety, World Electr. Veh. J. 3 (1) (2009) 17–26.
[9] N. Mutoh, Y. Takahashi, Y. Tomita, Failsafe drive performance of FRID electric vehicles with the structure driven by the front and rear wheels independently, IEEE Trans. Ind. Electron. 55 (6) (2008) 2306–2315.
[10] Q. Zheng, S. Tian, Q. Zhang, Optimal torque split strategy of dual-motor electric vehicle using adaptive nonlinear particle swarm optimization, Math. Probl. Eng. 2020 (2020).
[11] A. Hajduga, The torque distribution analysis for dual motor-single shaft electric drive. 2018 23rd International Conference on Methods & Models in Automation & Robotics (MMAR), IEEE, 2018, pp. 622–627.
[12] Z. Wang, J. Zhou, G. Rizzoni, A review of architectures and control strategies of dual-motor coupling powertrain systems for battery electric vehicles, Renew. Sustain. Energy Rev. 162 (2022) 112455.
[13] M. Hu, J. Zeng, S. Xu, C. Fu, D. Qin, Efficiency study of a dual-motor coupling EV powertrain, IEEE Trans. Veh. Technol. 64 (6) (2014) 2252–2260.
[14] J. Ruan, Q. Song, A novel dual-motor two-speed direct drive battery electric vehicle drivetrain, IEEE Access 7 (2019) 54330–54342, https://doi.org/10.1109/ACCESS.2019.2912994.
[15] B. Zhu, N. Zhang, P. Walker, W. Zhan, W. Yueyuan, N. Ke, X. Zhou, Two Motor Two Speed Power-Train System Research of Pure Electric Vehicle. Technical Report, SAE Technical Paper, 2013.
[16] M.V. Castro, S. Mukundan, C.L. Filho, G. Byczynski, B. Minaker, J. Tjong, N.C. Kar, A review of existing multi-motor electric powertrain sizing strategies. 2021 24th International Conference on Electrical Machines and Systems (ICEMS), 2021, pp. 2419–2424, https://doi.org/10.23919/ICEMS52562.2021.9634221.
[17] N. Mutoh, T. Kazama, K. Takita, Driving characteristics of an electric vehicle system with independently driven front and rear wheels, IEEE Trans. Ind. Electron. 53 (3) (2006) 803–813.
[18] U.R. Muduli, A.R. Beig, K.A. Jaafari, J.Y. Alsawalhi, R.K. Behera, Interrupt-free operation of dual-motor four-wheel drive electric vehicle under inverter failure, IEEE Trans. Transp. Electrif. 7 (1) (2021) 329–338, https://doi.org/10.1109/TTE.2020.2997354.

[19] C.P. Gor, V.A. Shah, M.P. Gor, Electric vehicle drive selection related issues. 2016 International Conference on Signal Processing, Communication, Power and Embedded System (SCOPES), IEEE, 2016, pp. 74–79.
[20] P. Jandura, J. Břoušek, M. Bukvic, The concept of a highly efficient powertrain for an electric vehicle with respect to vehicle driving dynamics. 2015 International Conference on Electrical Drives and Power Electronics (EDPE), IEEE, 2015, pp. 422–429.
[21] U. Vollmer, U. Schäfer, An at-all operating points highly efficient PMSM for HEV, World Electr. Veh. J. 2 (4) (2008) 334–342.
[22] D. Wu, Y. Li, J. Zhang, C. Du, Torque distribution of a four in-wheel motors electric vehicle based on a PMSM system model, Proc. Inst. Mech. Eng. Part D J. Autom. Eng. 232 (13) (2018) 1828–1845.
[23] E.A. Grunditz, T. Thiringer, Performance analysis of current BEVs based on a comprehensive review of specifications, IEEE Trans. Transp. Electrif. 2 (3) (2016) 270–289.
[24] B. Sun, S. Gao, C. Ma, J. Li, System power loss optimization of electric vehicle driven by front and rear induction motors, Int. J. Automot. Technol. 19 (1) (2018) 121–134.
[25] X. Yuan, J. Wang, Torque distribution strategy for a front-and rear-wheel-driven electric vehicle, IEEE Trans. Veh. Technol. 61 (8) (2012) 3365–3374.
[26] M.V. Castro, S. Mukundan, C.L. Filho, G. Byczynski, B. Minaker, J. Tjong, N. Kar, Non–dominated sorting genetic algorithm based determination of optimal torque–split ratio for a dual–motor electric vehicle. IECON 2021 – 47th Annual Conference of the IEEE Industrial Electronics Society, 2021, pp. 1–6, https://doi.org/10.1109/IECON48115.2021.9589555.
[27] X. Qi, Q. Wang, F. Xie, J. Cao, L. Chen, Q. Zhan, Researching of efficiency optimized torque distribution based on front and rear wheel independently drive electrical vehicle. 2016 19th International Conference on Electrical Machines and Systems (ICEMS), IEEE, 2016, pp. 1–6.
[28] Z. Yang, J. Wang, G. Gao, X. Shi, Research on optimized torque-distribution control method for front/rear axle electric wheel loader, Math. Probl. Eng. 2017 (2017).
[29] M. Hu, J. Zeng, S. Xu, C. Fu, D. Qin, Efficiency study of a dual-motor coupling EV powertrain, IEEE Trans. Veh. Technol. 64 (6) (2015) 2252–2260, https://doi.org/10.1109/TVT.2014.2347349.
[30] K. Yu, T. Lu, N. Yan, On-demand 4WD control of electric vehicles based on electric disconnect differential. Journal of Physics: Conference Series Vol. 2256, IOP Publishing, 2022, p. 012042.
[31] W. Da, W. Bo, Research on driving force optimal distribution and fuzzy decision control system for a dual-motor electric vehicle. 2015 34th Chinese Control Conference (CCC), IEEE, 2015, pp. 8146–8153.
[32] X. Hu, Y. Li, C. Lv, Y. Liu, Optimal energy management and sizing of a dual motor-driven electric powertrain, IEEE Trans. Power Electron. 34 (8) (2019) 7489–7501, https://doi.org/10.1109/TPEL.2018.2879225.
[33] M. Popescu, J. Goss, D.A. Staton, D. Hawkins, Y.C. Chong, A. Boglietti, Electrical vehicles–practical solutions for power traction motor systems, IEEE Trans. Ind. Appl. 54 (3) (2018) 2751–2762, https://doi.org/10.1109/TIA.2018.2792459.
[34] C. Du-Bar, O. Wallmark, Eddy current losses in a hairpin winding for an automotive application. 2018 XIII International Conference on Electrical Machines (ICEM), 2018, pp. 710–716, https://doi.org/10.1109/ICELMACH.2018.8507265.
[35] X. Lai, S. Wang, S. Ma, J. Xie, Y. Zheng, Parameter sensitivity analysis and simplification of equivalent circuit model for the state of charge of lithium-ion batteries, Electrochim. Acta 330 (2020) 135239.
[36] J. Estaller, A. Kersten, M. Kuder, A. Mashayekh, J. Buberger, T. Thiringer, R. Eckerle, T. Weyh, Battery impedance modeling and comprehensive comparisons of state-of-the-art cylindrical 18650 battery cells considering cells price, impedance, specific energy and C-rate. 2021 IEEE International Conference on Environment and Electrical Engineering and 2021 IEEE Industrial and Commercial Power Systems Europe (EEEIC/I&CPS Europe), 2021, pp. 1–8, https://doi.org/10.1109/EEEIC/ICPSEurope51590.2021.9584562.
[37] J. Estaller, A. Kersten, M. Kuder, T. Thiringer, R. Eckerle, T. Weyh, Overview of battery impedance modeling including detailed state-of-the-art cylindrical 18650 lithium-ion battery cell comparisons, Energies 15 (10) (2022) 3822.
[38] S. Sun, M. Gong, B. Wu, Y. Zou, Research on optimal meshing speed difference based on shift success probability for dog clutch in automated manual transmission. IOP Conference Series: Materials Science and Engineering Vol. 892, IOP Publishing, 2020, p. 012052.
[39] G. Bóka, J. Márialigeti, L. Lovas, B. Trencséni, Face dog clutch engagement at low mismatch speed, Periodica Polytechnica Transp. Eng. 38 (1) (2010) 29–35.
[40] C. Guo, C. Fu, R. Luo, G. Yang, Energy-oriented car-following control for a front- and rear-independent-drive electric vehicle platoon, Energy 257 (2022) 124732.
[41] H.A. Yavasoglu, J. Shen, C. Shi, M. Gokasan, A. Khaligh, Power split control strategy for an EV powertrain with two propulsion machines, IEEE Trans. Transp. Electrif. 1 (4) (2015) 382–390, https://doi.org/10.1109/TTE.2015.2504406.
[42] C. Du, S. Huang, Y. Jiang, D. Wu, Y. Li, Optimization of energy management strategy for fuel cell hybrid electric vehicles based on dynamic programming, Energies 15 (12) (2022) 4325.
[43] C. Maino, D. Misul, A. Musa, E. Spessa, Optimal mesh discretization of the dynamic programming for hybrid electric vehicles, Appl. Energy 292 (2021) 116920.
[44] H. Dou, Y. Zhang, L. Fan, Design of optimized energy management strategy for all-wheel-drive electric vehicles, Appl. Sci. 11 (17) (2021) 8218.
[45] EV reviews, EV tech specs, 2023, https://www.myevreview.com (Accessed on 2023-02-03).